Supporting Information

Quantitative Molecular-Level Understanding of Electrochemical Aluminum-Ion Intercalation into a Crystalline Battery Electrode

Ankur L. Jadhav, Jeffrey H. Xu, Robert J. Messinger*

Department of Chemical Engineering, The City College of New York, CUNY, New York, NY 10031, United States

*E-mail: rmessinger@ccny.cuny.edu

Methods

Chevrel Mo_6S_8 synthesis. $Cu_2Mo_6S_8$ was synthesized via a solid-state route as reported by Partha et al.[1] In a typical synthesis, 1.2 g molybdenum powder (Mo, Alfa Aesar, 99.9%), 0.8 g copper sulfide (CuS, Alfa Aesar, 99.9%) and 2 g molybdenum disulfide (MoS_2, Alfa Aesar, 99.9%) were ball-milled for 3 h and the mixture was placed in a tube furnace at 1000 °C for 7 h under argon flow to generate $Cu_2Mo_6S_8$. To generate Mo_6S_8, the $Cu_2Mo_6S_8$ powder was then mixed with 6 M HCl solution for 8 h at room temperature under constant air bubbling. The solution was filtered, rinsed three times with ethanol and deionized water, and dried in a vacuum oven at 90 °C overnight.

Composite electrode preparation. To prepare composite electrodes, chevrel Mo_6S_8 (80 wt%) and carbon black (10 wt %) (Super-P, Alfa Aesar, 99%) were ball-milled in the glovebox for 1 h. In a glass vial, polyvinylidene fluoride (PVDF) binder (10 wt%) (Sigma Aldrich, average molecular weight 534000 g/mol) was dissolved in N-methyl-2-pyrrolidone (NMP) and the ball-milled Mo_6S_8-carbon black mixture was then added to the solution. The mixture was agitated with a vortex mixer for 5 min and ultrasonicated for 30 s to form a slurry, which was then pasted on molybdenum foil (0.025 mm, Alfa Aesar, 99.95%) using a doctor blade. The electrode was dried in a vacuum oven at 120 °C overnight to evaporate the NMP solvent. The final electrode thickness was ca. 80 μm.

Cell Assembly. All cells were constructed in an argon-filled glovebox with H_2O and O_2 levels below 1 ppm. Polytetrafluorethylene (PTFE) Swagelok unions with diameters of ¼-in (6.35 mm) or ½-in (12.70 mm) were used to assemble airtight cells. Molybdenum rods were used as current collectors for both electrodes. A glass microfiber filter (GF/D, Whatman) was used as a separator. Aluminum foil (MTI, 99.99%, 0.1 mm thickness) was used as anode. A Lewis acidic mixture of aluminum chloride/1-ethyl-3-methylimidazolium chloride ($AlCl_3$:[Emim]Cl), molar ratio 1.5:1) was used as the electrolyte. 40 μL and 120 μL of electrolyte were added to the ¼-in and ½-in Swagelok cells, respectively.

Electrochemical Measurements. Galvanostatic cycling and galvanostatic intermittent titration technique (GITT) measurements were performed on an Arbin LBT battery tester. For GITT measurements, a constant current pulse (10 mA/g) of 15 min was followed by a rest time of 2 h, during which the potential reached equilibrium. Cyclic voltammetry (CV) measurements were performed on a Metrohm Autolab potentiostat (PGSTAT302N) using scan rates of 20 μV/s. The open circuit potential (OCP) of Al-Mo_6S_8 cells was ca. 1.6 V. For all electrochemical measurements, the upper and lower cut-off potentials were 1.2 V and 0.05 V, respectively.

Sample Preparation. After electrochemical measurements, cells were disassembled in an argon-filled glovebox. The electrodes were harvested and rinsed three times with anhydrous methanol for *ex situ* analyses. For "untreated" samples, excess electrolyte was removed from the electrode surface by blotting dry with a Kimwipe instead of rinsing with solvent. The electrodes were then scraped off of the molybdenum foil current collectors. For solid-state NMR measurements, the samples were crushed and packed into 1.6-mm zirconia rotors inside an argon-filled glovebox.

Solid-state NMR Spectroscopy. Solid-state NMR spectra were acquired on a Bruker AVANCE III HD 600 NMR spectrometer with a 14.1 T narrow-bore superconducting magnet operating at 156.375 MHz for ^{27}Al nuclei. A PhoenixNMR 1.6-mm HXY MAS probehead was used, where all measurements were conducted with magic-angle-spinning (MAS) rates of 20 kHz. Air at a temperature of 293.2 K was pumped through the probehead at 600 L/h to mitigate sample heating due to MAS. ^{27}Al shifts were referenced to 1 M aqueous $Al(NO_3)_3$ at 0 ppm.

All solid-state ^{27}Al single-pulse MAS NMR experiments were calibrated to be quantitative by using (i) short radiofrequency (rf) pulses ($\pi/12$) within the linear excitation regime for quadrupolar spin-5/2 nuclei and (ii) recycle delays (0.1 s) such that all ^{27}Al spins relaxed to thermal equilibrium ($> 5*T_1$, the longitudinal relaxation time). For quadrupolar nuclei, the solid-state NMR signals of moieties with different quadrupolar frequencies (ω_Q) may nutate at different rates, depending on the rf field strength (ω_1).[2,3] For half-integer quadrupolar nuclei with spin quantum number I, non-selective ($\omega_Q/\omega_1 << 1$) or central-transition selective ($\omega_Q/\omega_1 >> 1$) rf pulses of nuclei will result in NMR signals that have maximum signal intensities at flip angles Φ of $\pi/2$ or $\pi/[2(I+1/2)]$, respectively. To ensure uniform excitation of all half-integer spins within a linear regime, regardless of their quadrupolar frequencies ω_Q, the optimal flip angle is[2]

$$\Phi = t_p \omega_1 \leq \pi/[4(I+1/2)],$$

where t_p is the rf pulse length. The optimal flip angle for quantitative ^{27}Al (I = 5/2) NMR measurements is thus $\pi/12$. Here, all solid-state ^{27}Al NMR experiments were performed with $\pi/12$ pulse lengths of 0.317 μs, which were calculated based on the optimum $\pi/2$ pulse length of 1.90 μs (rf field strength υ_1 of 132 kHz) of 1 M aqueous $Al(NO_3)_3$. All spectra were deconvoluted using the DMFit program.[4]

To quantify the total amount of intercalated aluminum ions ($Al_xMo_6S_8$), the absolute integrated ^{27}Al signal intensities of Al-ions within both cavities were normalized by sample mass. The total ^{27}Al signal area associated with intercalated aluminum ions for the fully intercalated (discharged) sample was equated to a composition of $Al_{4/3}Mo_6S_8$, while the composition of the other electrode samples in the series were determined by scaling the absolute integrated ^{27}Al signal intensity of intercalated aluminum ions, normalized by sample mass, to that of the fully intercalated $Al_{4/3}Mo_6S_8$ composition. The $Al_xMo_6S_8$ compositions determined from NMR results are in excellent agreement with the expected theoretical compositions (Table 1, main manuscript).

X-ray diffraction. A PANalytical X'pert Pro powder diffractometer with a Cu-Kα radiation source (λ= 0.544 nm) was used to characterize chevrel crystal structures. A scan rate of 0.8 (° 2θ/min) was used to scan a 2θ range of 10° to 60°.

Scanning electron microscopy. A Zeiss Supra VP 55 scanning electron microscope was used to image the morphology of the chevrel particles.

Supporting Figures & Text

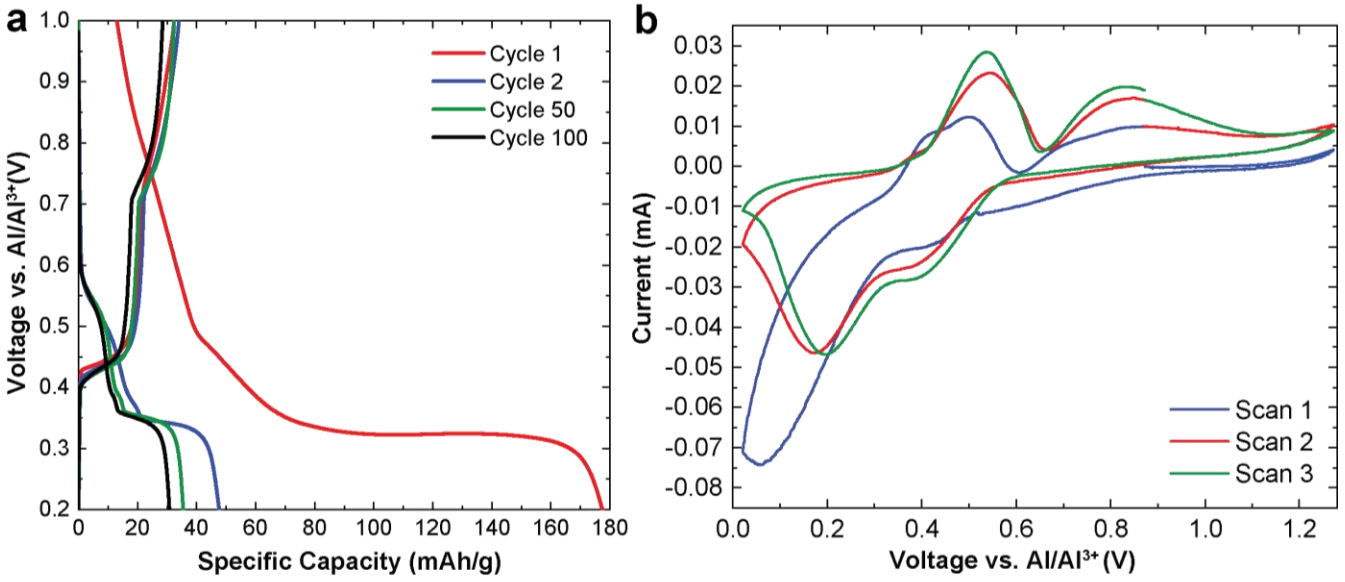

Figure S1: Electrochemical cycling of Al-Mo_6S_8 cells at 25 °C. (a) Galvanostatic cycling performed at 10 mA/g and (b) cyclic voltammetry conducted at 50 μV/s.

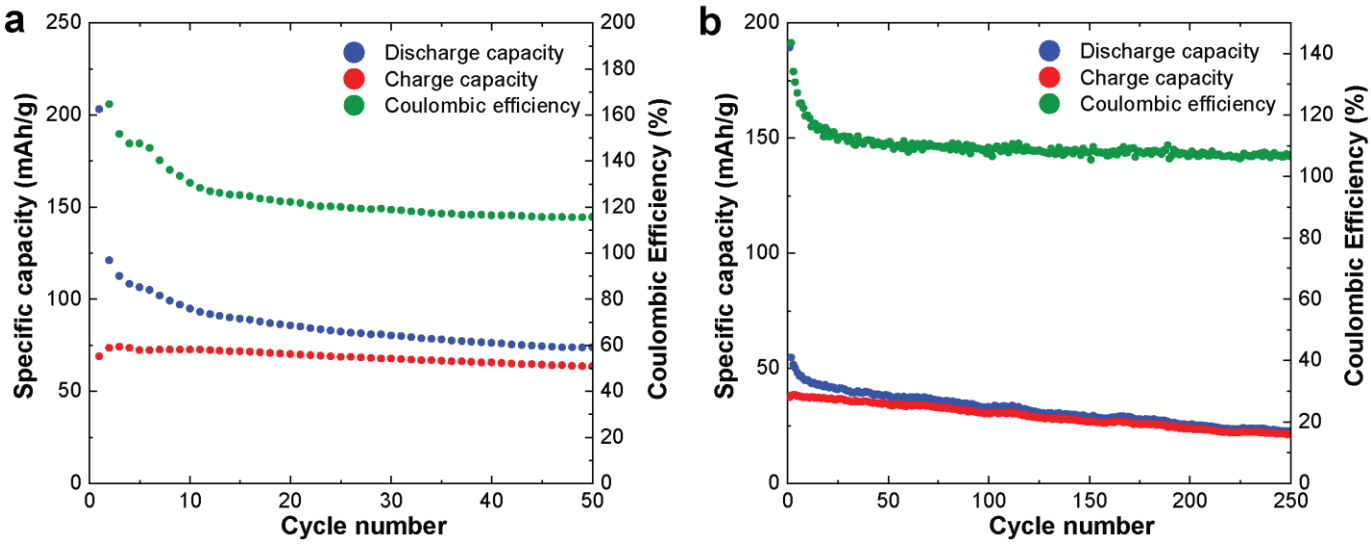

Figure S2: Specific capacities and Coulombic efficiencies during extended galvanostatic cycling of Al-Mo_6S_8 cells conducted at 10 mA/g and temperatures of (a) 50 °C and (b) 25 °C.

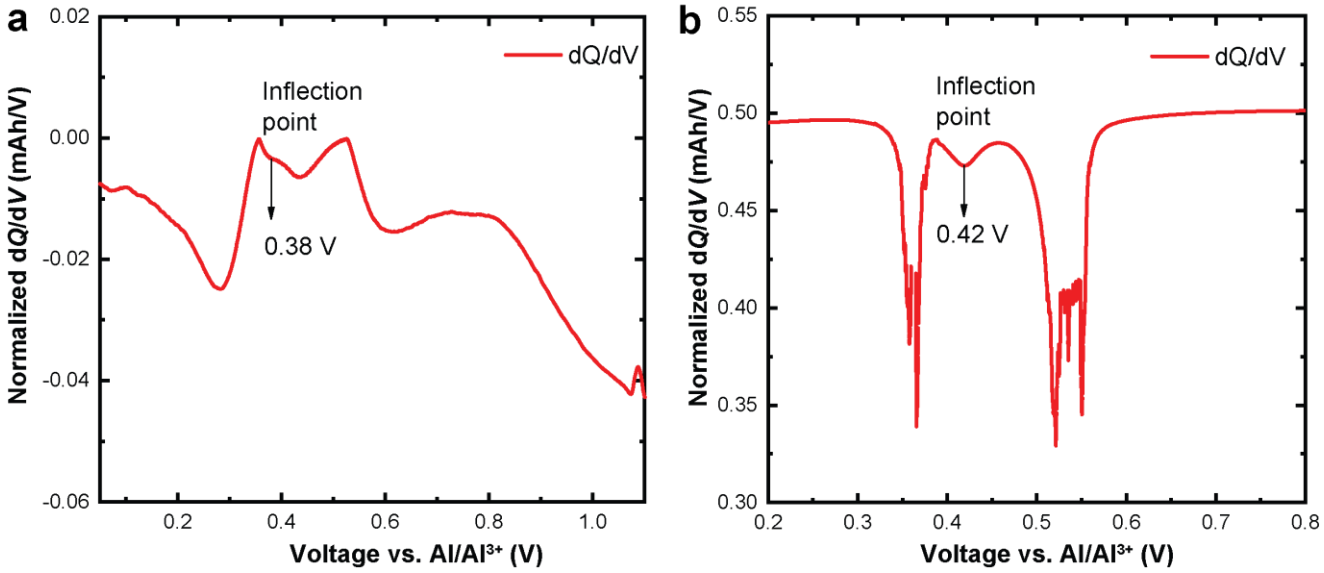

Figure S3: Differential capacity (d*Q*/d*V*) plots of galvanostatic discharge of Al-Mo_6S_8 cells cycled at 50 °C during the (a) first and (b) second discharge. The inflection points at (a) 0.38 V and (b) 0.42 V correspond to the minor reduction peak between the two prominent reduction peaks in the CV scans shown in Figure 1b.

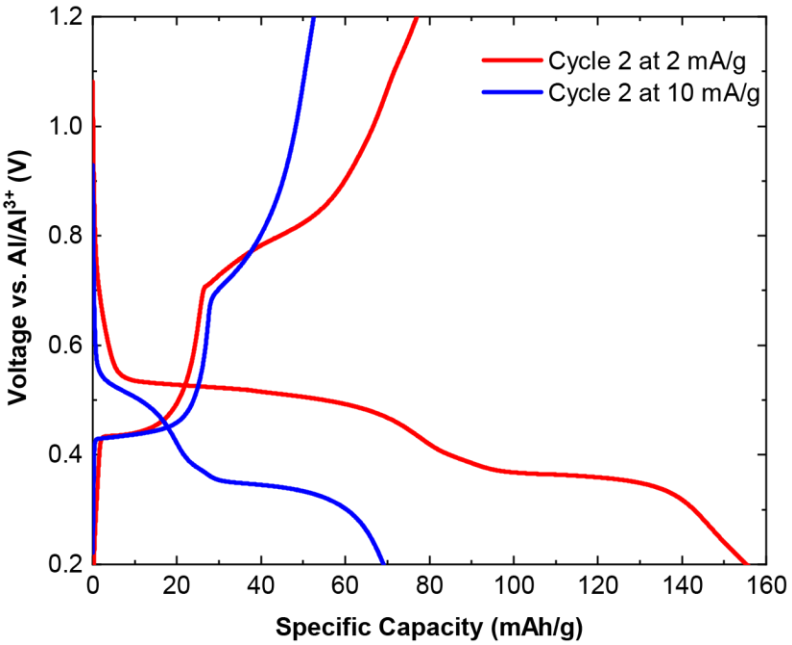

Figure S4: Galvanostatic cycling (second cycle) of Al-Mo_6S_8 cells performed at 25 °C and current densities of 2 mA/g (red) and 10 mA/g (blue). The results show that Al-ion intercalation associated with the first discharge plateau is diffusion limited. The extra capacity beyond 128 mAh/g observed in the battery discharged at 10 mA/g, which mainly occurs at low potentials (<0.38 V), may be due to electrolyte degradation or other irreversible side reactions.

Text S1: Calculation of aluminum-ion diffusion coefficients using GITT measurements

In the Galvanostatic Intermittent Titration Technique (GITT), a constant current pulse is applied followed by a rest step that is sufficiently long such that the system relaxes to its thermodynamic equilibrium potential[5]. Repeating this process enables the equilibrium potential to be determined during the charge-discharge process, as well as the overpotential that occurs during the constant current measurement.

Assuming one-dimensional Fickian diffusion, Wen et al[6]. derived the following equation for the diffusion coefficient of an electroactive ion intercalating into a crystalline solid host material:

$$D_{ion} = \frac{4}{\pi}\left(\frac{IV_M}{Z_A FS}\right)^2 \left[\frac{dE(\delta)}{d\delta} \Big/ \frac{dE(t)}{d\sqrt{t}}\right]^2$$

Assuming a linear relationship between $dE(\delta)$ and $d\delta$, this equation can be simplified to

$$D_{ion} \cong \frac{4}{\pi}\left(\frac{IV_M}{Z_A FS}\right)^2 [\Delta Es/\Delta Et]^2$$

where D_{ion} is ion diffusion coefficient, I is the current applied during a pulse, V_M is the molar volume , Z_A is charge valence, F is Faraday's constant, S is the surface area of the electrode-electrolyte interface, ΔE_s is the change in steady-state potential during the rest time, ΔE_t is the change in the potential measured during the current pulse. Here, pulses with I = 10 mA/g were used with a rest time of 2 h between current pulses. V_m = 160 cm^3/mol for Mo_6S_8, Z_A = 3 for Al^{3+}, and S = 10.95 m^2/g on the pristine Mo_6S_8 as measured by BET analysis of an N_2 adsorption isotherm. The results yielding $D_{Al^{3+}} \sim 10^{-18}$ cm^2/s for the first plateau and $D_{Al^{3+}} \sim 10^{-16}$ cm^2/s for the second plateau (e.g., see Fig. 1, main manuscript, second discharge cycle, and Fig. S4, first discharge cycle).

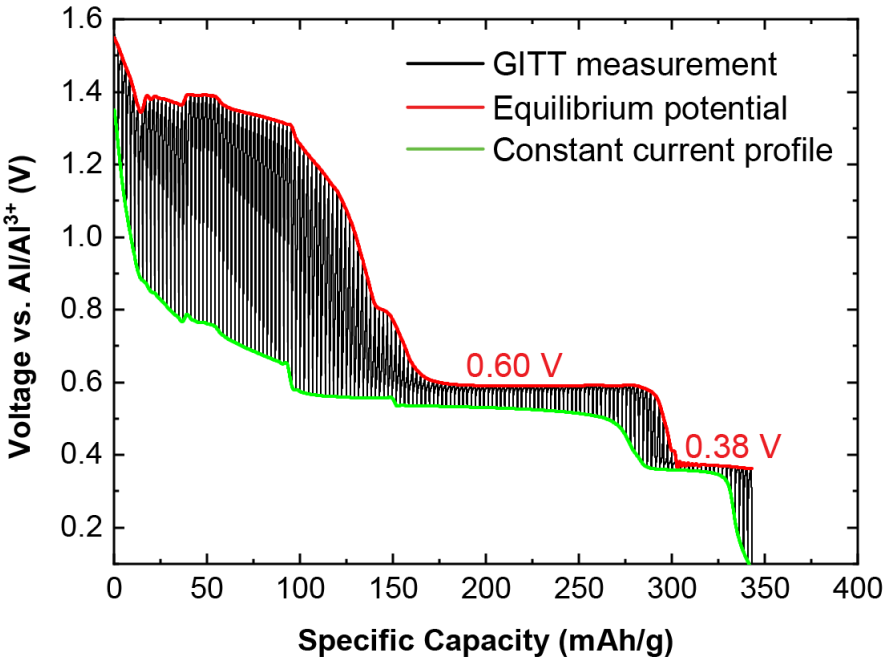

Figure S5: GITT measurement of the first discharge of an Al-Mo_6S_8 cell conducted at 50 °C. Note the equilibrium potentials and large overpotentials associated with the initial electrolyte decomposition reactions.

Text S2: Crystal structure and morphology of pristine and cycled Mo_6S_8 electrodes.

The chloroaluminate-containing $AlCl_3$:[EMIm]Cl ionic liquid electrolytes are corrosive and have been shown to react with proposed electrode materials, such V_2O_5,[7,8] as shown by Wen et al.[9] Thus, it is important to ensure that the observed current is indeed due to Al^{3+} intercalation and not from undesired electrochemical reactions or irreversible electrode degradation processes. Chevrel electrodes were characterized by *ex situ* XRD and SEM to ensure that the crystal structure and morphology remained intact upon cycling. XRD measurements (Figure S6a) were performed on pristine (Mo_6S_8), discharged ($Al_{4/3}Mo_6S_8$), and charged electrodes (Mo_6S_8), respectively. After discharge, Al^{3+} ions intercalate within the chevrel Mo_6S_8, altering the reflections between 2θ value of 30˚ and 47˚ as observed previously by Lee et al.[10], indicating changes in crystal structure upon intercalation.[11] The XRD reflections also broaden, which may be a result of local volume expansions of the framework associated with the stress of intercalating highly charged Al^{3+} ions.[12] After charging, when Al^{3+} ions have deintercalated from the chevrel, the XRD reflections are similar those of the pristine material, indicating the reversibility of the Al-ion intercalation process.

SEM images of pristine and discharged electrodes (Figure S6b and S6c, respectively) establish no change in the cubic morphology of the chevrel Mo_6S_8 particles. If the electrochemical reaction were a conversion process that involved breaking and forming chemical bonds, the electrodes would be expected to dissolve and recrystallize, resulting in a change of particle morphology of the electrode particles[13]. The cubic morphology remains intact, however, consistent with a reversible aluminum-ion intercalation process.

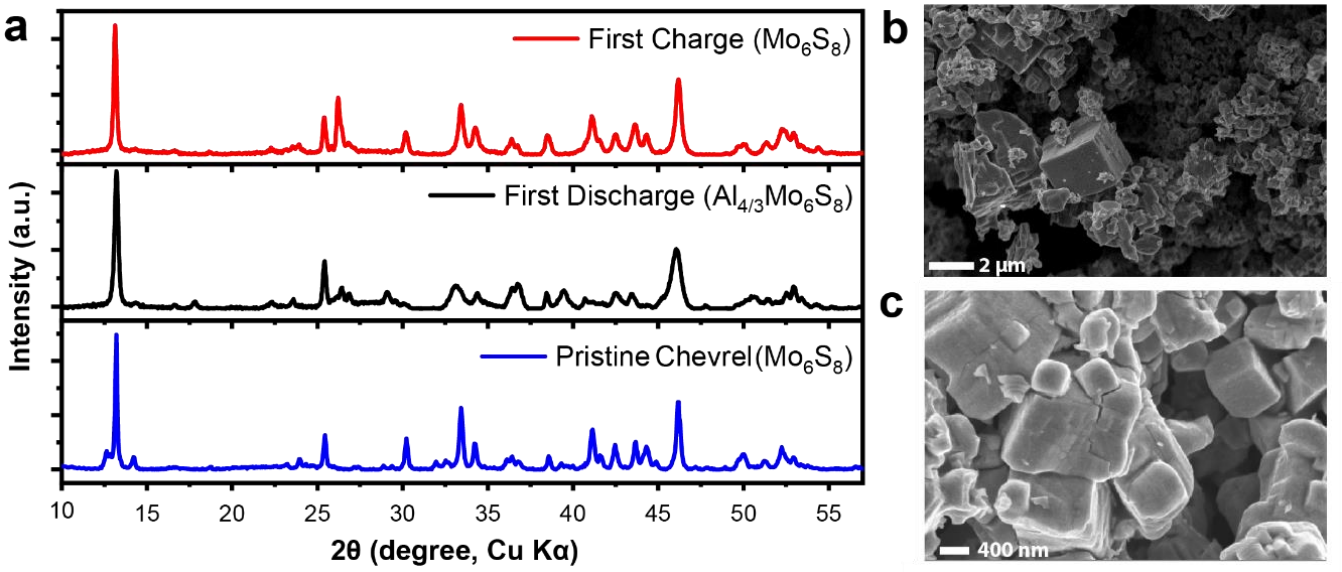

Figure S6: Crystal structure and morphology of chevrel Mo_6S_8 electrodes upon Al-ion intercalation. (a) XRD measurements on electrodes at specified states-of-charge. SEM images of (b) pristine Mo_6S_8 and (c) an Mo_6S_8 electrode after the first discharge. The results establish that the crystal structure and morphology of Mo_6S_8 are preserved upon electrochemical cycling.

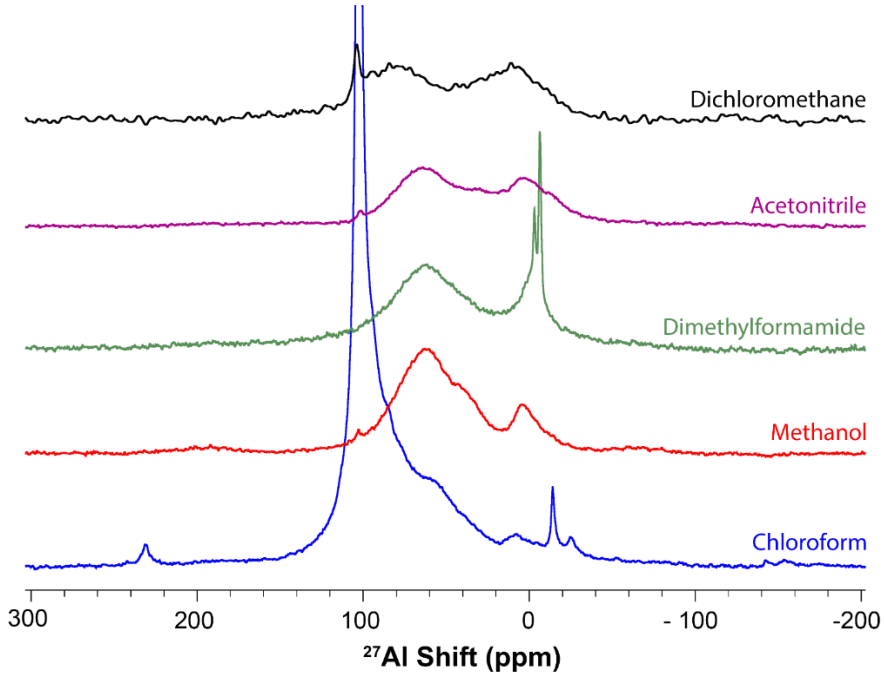

Figure S7: Solid-state ^{27}Al single-pulse MAS NMR spectra of discharged (fully intercalated) $Al_{4/3}Mo_6S_8$ electrodes rinsed with different solvents, acquired using $\pi/12$ rf pulses under conditions of 20 kHz MAS and 14.1 T. The Al-Mo_6S_8 cells were discharged at 10 mA/g and 50 °C. Chloroform was the least effective in removing the chloroaluminate-containing ionic liquid electrolyte. Rinsing with dimethylformamide and chloroform both resulted in the formation of additional ^{27}Al species, whose NMR shifts are consistent with octahedrally-coordinated environments.

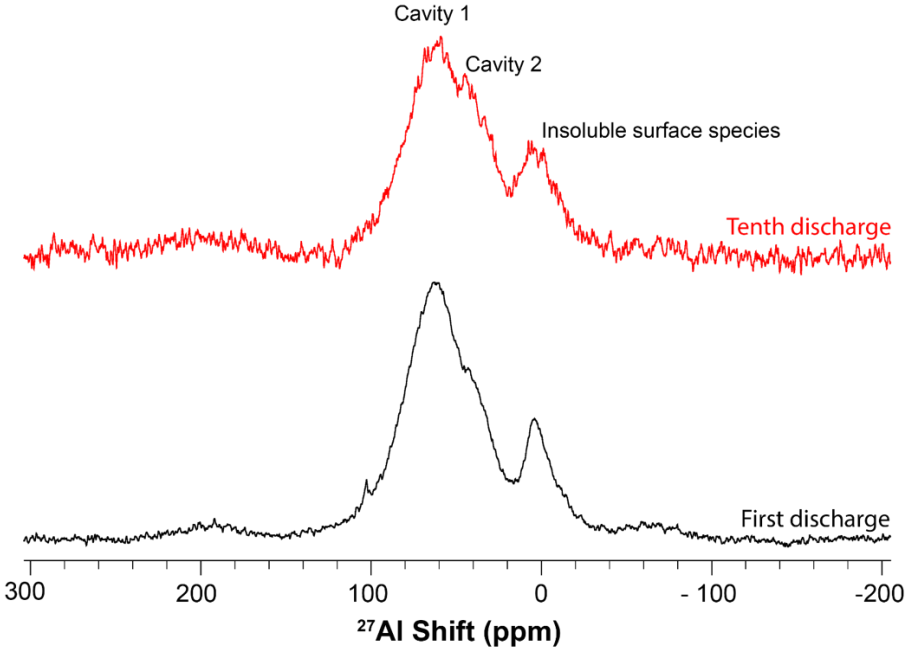

Figure S8: Solid-state ^{27}Al single-pulse MAS NMR spectra of $Al_{4/3}Mo_6S_8$ electrodes acquired after the first (blue) and tenth (red) discharge, acquired using $\pi/12$ rf pulses under conditions of 20 kHz MAS and 14.1 T. The Al-Mo_6S_8 cells were cycled at 10 mA/g and 50 °C. The electrodes were rinsed with anhydrous methanol prior to NMR measurements. This result not only indicates the reversibility of the intercalation process, but also establishes that no other discharge products (e.g., amorphous surface species) accumulate over time.

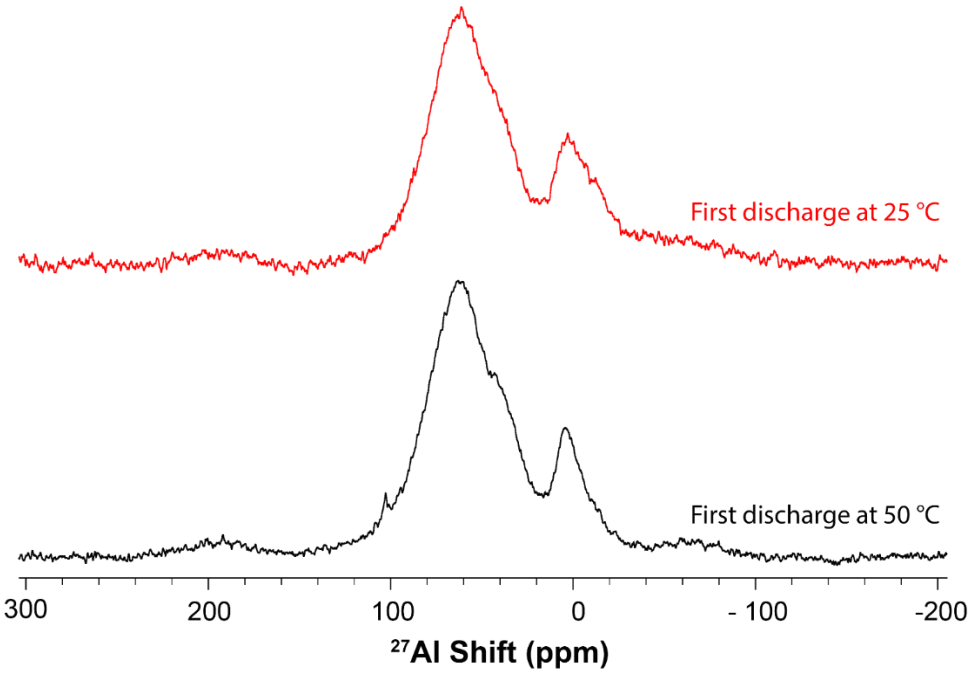

Figure S9: Solid-state ^{27}Al single-pulse MAS NMR spectra of $Al_{4/3}Mo_6S_8$ electrodes acquired after the first discharge at temperature of 25 °C (red) and 50 °C (blue), acquired using $\pi/12$ rf pulses under conditions of 20 kHz MAS and 14.1 T. The Al-Mo_6S_8 cells were cycled at 10 mA/g. Electrodes were rinsed with methanol prior to NMR measurements. The solid-state NMR measurements show ^{27}Al signals associated with intercalated aluminum ions that are identical in shift and relative population (within experimental error).

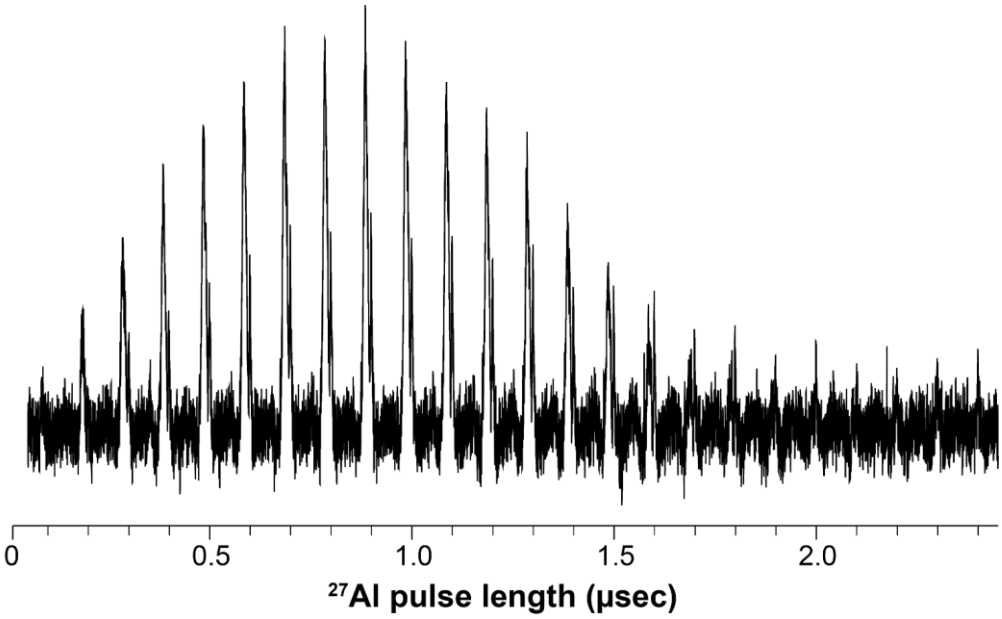

Figure S10: Solid-state ^{27}Al single-pulse MAS NMR measurements on a discharged (fully intercalated) $Al_{4/3}Mo_6S_8$ electrode as a function of rf pulse length at a fixed power level, acquired under conditions of 20 kHz MAS and 14.1 T. The ^{27}Al NMR signals associated with intercalated Al ions could not be inverted.

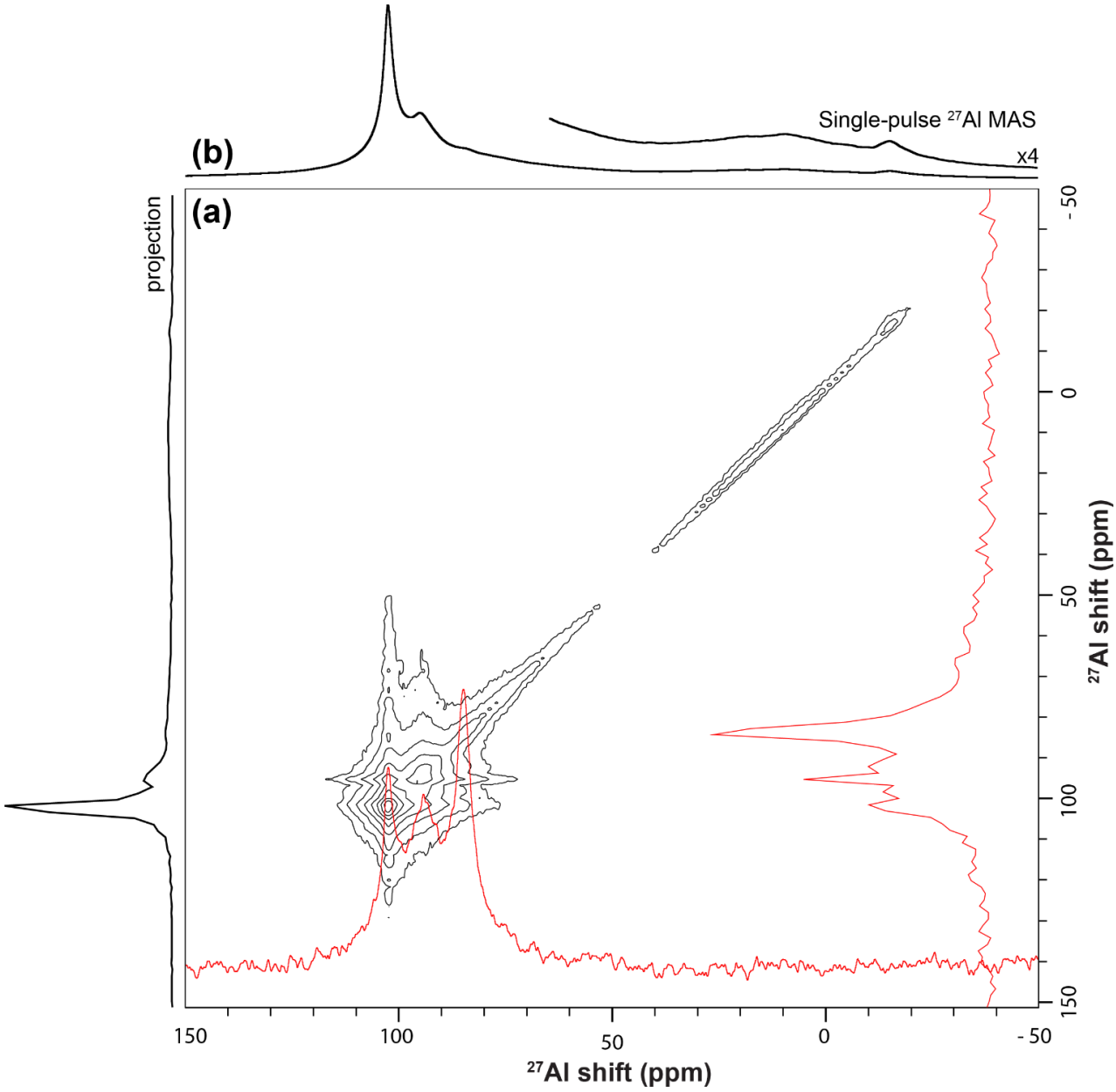

Figure S11: (a) Solid-state 2D ^{27}Al{^{27}Al} exchange spectroscopy (EXSY) NMR spectrum on an untreated, fully intercalated $Al_{4/3}Mo_6S_8$ electrode after first discharge, acquired under conditions of 20 kHz MAS and 14.1 T. A mixing time of 50 µs was used. Chemical exchange is observed between chloroaluminate species with ^{27}Al signals at 102.7 ppm, 97.2 ppm and 84.4 ppm, which are associated with $AlCl_4$-, $Al_2Cl_7^-$, and an unknown aluminum-containing species in the electrolyte. The 2D EXSY NMR spectrum establishes that these ^{27}Al signals are in the liquid phase. The 1D spectra shown in red are slices from the 2D spectrum taken at 84.4 ppm in both dimensions. (b) A separately acquired solid-state ^{27}Al single-pulse MAS NMR spectrum is displayed along the horizontal axes.

References

(1) Saha, P.; Jampani, P. H.; Datta, M. K.; Hong, D.; Gattu, B.; Patel, P.; Kadakia, K. S.; Manivannan, A.; Kumta, P. N. A Rapid Solid-State Synthesis of Electrochemically Active Chevrel Phases (Mo_6T_8; T = S, Se) for Rechargeable Magnesium Batteries. *Nano Res.* **2017**, *10* (12), 4415–4435.

(2) Fenzke, D.; Freude, D.; Fröhlich, T.; Haase, J. NMR Intensity Measurements of Half-Integer Quadrupole Nuclei. *Chem. Phys. Lett.* **1984**, *111* (1–2), 171–175.

(3) Samoson, A.; Lippmaa, E. Excitation Phenomena and Line Intensities in High-Resolution NMR Powder Spectra of Half-Integer Quadrupolar Nuclei. *Phys. Rev. B* **1983**, *28* (11), 6567.

(4) Massiot, D.; Fayon, F.; Capron, M.; King, I.; Le Calvé, S.; Alonso, B.; Durand, J. O.; Bujoli, B.; Gan, Z.; Hoatson, G. Modelling One- and Two-Dimensional Solid-State NMR Spectra. *Magn. Reson. Chem.* **2002**, *40* (1), 70–76.

(5) Zhu, Y.; Gao, T.; Fan, X.; Han, F.; Wang, C. Electrochemical Techniques for Intercalation Electrode Materials in Rechargeable Batteries. *Acc. Chem. Res.* **2017**, *50* (4), 1022–1031.

(6) Wen, C. J. Thermodynamic and Mass Transport Properties of "LiAl." *J. Electrochem. Soc.* **1979**, *126* (12), 2258.

(7) Gu, S.; Wang, H.; Wu, C.; Bai, Y.; Li, H.; Wu, F. Confirming Reversible Al^{3+} Storage Mechanism through Intercalation of Al^{3+} into V_2O_5 Nanowires in a Rechargeable Aluminum Battery. *Energy Storage Mater.* **2017**, *6*, 9–17.

(8) Wang, H.; Bai, Y.; Chen, S.; Luo, X.; Wu, C.; Wu, F.; Lu, J.; Amine, K. Binder-Free V_2O_5 Cathode for Greener Rechargeable Aluminum Battery. *ACS Appl. Mater. Interfaces* **2015**, *7* (1), 80–84.

(9) Wen, X.; Liu, Y.; Jadhav, A.; Zhang, J.; Borchardt, D.; Shi, J.; Wong, B. M.; Sanyal, B.; Messinger, R. J.; Guo, J. Materials Compatibility in Rechargeable Aluminum Batteries: Chemical and Electrochemical Properties between Vanadium Pentoxide and Chloroaluminate Ionic Liquids. *Chem. Mater.* **2019**, *31* (18), 7238–7247.

(10) Lee, B.; Lee, H. R.; Yim, T.; Kim, J. H.; Lee, J. G.; Chung, K. Y.; Cho, B. W.; Oh, S. H. Investigation on the Structural Evolutions during the Insertion of Aluminum Ions into Mo_6S_8 Chevrel Phase. *J. Electrochem. Soc.* **2016**, *163* (6), A1070–A1076.

(11) Geng, L.; Scheifers, J. P.; Zhang, J.; Bozhilov, K. N.; Fokwa, B. P. T.; Guo, J. Crystal Structure Transformation in Chevrel Phase Mo_6S_8 Induced by Aluminum Intercalation. *Chem. Mater.* **2018**, *30* (23), 8420–8425.

(12) Geng, L.; Lv, G.; Xing, X.; Guo, J. Reversible Electrochemical Intercalation of Aluminum in Mo_6S_8. *Chem. Mater.* **2015**, *27* (14), 4926–4929.

(13) Canepa, P.; Sai Gautam, G.; Hannah, D. C.; Malik, R.; Liu, M.; Gallagher, K. G.; Persson, K. A.; Ceder, G. Odyssey of Multivalent Cathode Materials: Open Questions and Future Challenges. *Chem. Rev.* **2017**, *117* (5), 4287–4341.